BIOLOGICAL CRYSTALLOGRAPHY
ISSN 1399-0047

The 1.65 Å resolution structure of the complex of AZD4547 with the kinase domain of FGFR1 displays exquisite molecular recognition

Yuliana Yosaatmadja,[a] Adam Vorn Patterson,[b,c] Jeff Bruce Smaill[b,c] and Christopher John Squire[a,c]*

[a]School of Biological Sciences, The University of Auckland, Private Bag 92019, Auckland, New Zealand, [b]Auckland Cancer Society Research Centre, Faculty of Medical and Health Sciences, The University of Auckland, Private Bag 92019, Auckland, New Zealand, and [c]Maurice Wilkins Centre for Molecular Biodiscovery, c/o The University of Auckland, Private Bag 92019, Auckland, New Zealand. *Correspondence e-mail: c.squire@auckland.ac.nz

Received 9 November 2014
Accepted 17 December 2014

Keywords: AZD4547; fibroblast growth factor receptor.

PDB reference: FGFR1 in complex with AZD4547, 4wun

Supporting information: this article has supporting information at journals.iucr.org/d

The fibroblast growth factor receptor (FGFR) family are expressed widely in normal tissues and play a role in tissue repair, inflammation, angiogenesis and development. However, aberrant signalling through this family can lead to cellular proliferation, evasion of apoptosis and induction of angiogenesis, which is implicated in the development of many cancers and also in drug resistance. The high frequency of FGFR amplification or mutation in multiple cancer types is such that this family has been targeted for the discovery of novel, selective drug compounds, with one of the most recently discovered being AZD4547, a subnanomolar (IC_{50}) FGFR1 inhibitor developed by AstraZeneca and currently in clinical trials. The 1.65 Å resolution crystal structure of AZD4547 bound to the kinase domain of FGFR1 has been determined and reveals extensive drug–protein interactions, an integral network of water molecules and the tight closure of the FGFR1 P-loop to form a long, narrow crevice in which the AZD4547 molecule binds.

1. Introduction

The fibroblast growth factor receptor (FGFR) family consists of four highly conserved receptor tyrosine kinases (RTKs) termed FGFR1–4 (Zhang *et al.*, 2006). Similar to other well characterized RTKs such as the epidermal growth factor receptors (EGFRs), the platelet-derived growth factor receptors (PDGFRs) and the vascular endothelial growth factor receptors (VEGFRs), the FGFR family comprise an extracellular growth factor ligand-binding domain, a single-pass transmembrane domain and a carboxy-terminal cytoplasmic domain (Mohammadi *et al.*, 2005). Binding of one of the 18 known secreted FGF ligands leads to receptor dimerization, autophosphorylation and activation of downstream signalling pathways such as the MAPK-, STAT- and PI3K/AKT-regulated pathways (Klint & Claesson-Welsh, 1999; Hart *et al.*, 2000; Eswarakumar *et al.*, 2005). The FGF ligand and receptor families are expressed broadly in many normal tissues and play a critical role in normal physiology, including tissue repair, inflammation, haematopoiesis, angiogenesis and embryonic development (Beenken & Mohammadi, 2009; Turner & Grose, 2010).

Inappropriate signalling through the FGFR family leading to cellular proliferation, evasion of apoptosis and induction of angiogenesis has been implicated in the development and resistance of many cancers. Recent fluorescence *in situ* hybridization-based genetic analysis of tumours from 153 patients with smoking-related squamous-cell carcinoma, a

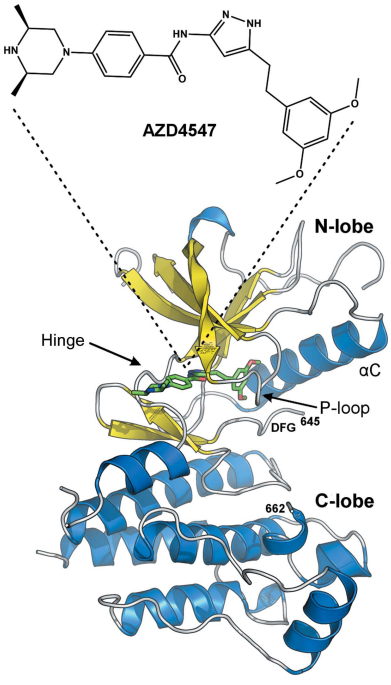

subtype of non-small-cell lung cancer, identified high-level amplifications of FGFR1 in 22% of patients (Weiss *et al.*, 2010). In addition, the FGFR pathway has also been identified as the major cause of resistance to chemotherapy in small-cell lung cancer, which is initially chemosensitive but recurs rapidly (Pardo *et al.*, 2002, 2003, 2006).

Outside of lung cancer, amplification and/or mutation of FGFR3 is observed in 50–60% of non-muscle invasive bladder cancers (Cappellen *et al.*, 1999). Upregulated FGFR1 expression is associated with the transition of hormone-naive to castrate-resistant prostate cancer (Armstrong *et al.*, 2011). Autocrine FGF2 signalling promotes the growth of 47% of triple-negative and 62% of basal-like breast cancer cell lines both *in vitro* and *in vivo* (Sharpe *et al.*, 2011). Indeed, gene amplification, activating mutation or chromosomal translocation of one or more members of the FGFR1–4 family has been implicated in the pathogenesis of lung, bladder, prostate, breast, ovarian, gastric, colorectal, endometrial and cervical cancers, such that the FGFR family has been described as one of the most frequently amplified or mutated molecular targets in oncology (Turner & Grose, 2010).

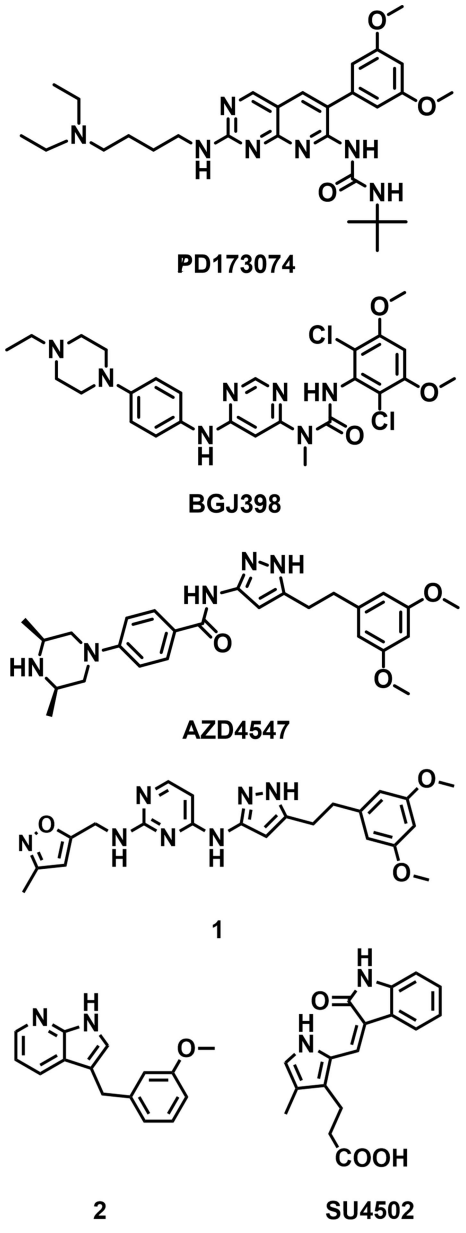

Figure 1
Molecular structures of PD173074, BGJ398, AZD4547, compound **1**, compound **2** and SU4502.

Large pharma interest in FGFR1–4 has seen several small-molecule tyrosine kinase inhibitors advance to human trials (Liang *et al.*, 2012; Dieci *et al.*, 2013). The most clinically advanced (phase III) are multikinase inhibitors with significant off-target potency against PDGFR, VEGFR and c-KIT, for example brivanib (Chou & Finn, 2012), dovitinib (Kim *et al.*, 2011), nintedanib (Ledermann *et al.*, 2011; Hilberg *et al.*, 2008) and pazopanib (Ray-Coquard & Thomas, 2012; Kasper & Hohenberger, 2011; Nieto *et al.*, 2011), likely resulting in increased side effects in clinical trials. More recently, FGFR-selective compounds such as BGJ398 and AZD4547 (from Novartis and AstraZeneca, respectively), illustrated in Fig. 1, have entered phase I/II clinical trials (Guagnano *et al.*, 2012; Gavine *et al.*, 2012; Brooks *et al.*, 2012).

The first inhibitor-bound FGFR1 crystal structure of the prototypic FGFR-selective inhibitor PD173074 (Fig. 1) was published in 1998 (Mohammadi *et al.*, 1998). Since then, structure-guided design of FGFR1–4 inhibitors has been widely utilized by several groups (Zhou *et al.*, 2010; Norman *et al.*, 2012). For example, the binding mode of BGJ398 to FGFR1 was recently reported in an inhibitor-bound crystal structure at 2.8 Å resolution (Guagnano *et al.*, 2012). As part of our own work towards the design of novel, selective FGFR1–4 inhibitors, we have been interested in FGFR1 biology and in determining ligand-bound structures as design guides. We here report the complex of AZD4547 bound to the kinase domain of FGFR1 at 1.65 Å resolution. The structure reveals the extensive AZD4547–FGFR1 interactions that include an integral network of water molecules and a tight closure of the FGFR1 P-loop, producing a long narrow crevice in which the drug molecule binds.

2. Materials and methods

2.1. Expression and purification

Chemical reagents were sourced as detailed in the Supporting Information. FGFR1 and PTP1B (phosphotyrosine phosphatase 1B) DNA sequences were codon-optimized for *Escherichia coli* expression and purchased from GeneArt subcloned into the pETDuet vector (Merck) using NdeI/KpnI and NcoI/HindIII for FGFR1 and PTP1B, respectively (sequence details are provided in the Supporting Information). The PTP1B sequence was cloned full length, while only the FGFR1 sequence corresponding to the kinase-domain amino-acid residues Gly459–Glu765 was cloned. In addition, two amino-acid mutations (C488A and C584S) were introduced into the sequence to prevent inappropriate disulfide formation in the recombinant protein preparation. The final constructs were sequence-confirmed. PTP1B is included in the

Table 1
Data collection and processing.

Values in parentheses are for the outer shell.

Diffraction source	MX2, AS
Wavelength (Å)	0.9537
Temperature (K)	100
Detector	ADSC Quantum 315r
Crystal-to-detector distance (mm)	200
Rotation range per image (°)	0.5
Total rotation range (°)	216
Exposure time per image (s)	1
Space group	*C*2
a, *b*, *c* (Å)	211.00, 51.31, 65.63
α, β, γ (°)	90, 106.99, 90
Mosaicity (°)	0.14
Resolution range (Å)	19.7–1.65 (1.68–1.65)
Total No. of reflections	361009 (17818)
No. of unique reflections	80820 (3956)
Completeness (%)	99.3 (99.9)
$R_{\rm merge}$	0.045 (0.818)
Multiplicity	4.5 (4.5)
$\langle I/\sigma(I)\rangle$	14.2 (1.7)
$CC_{1/2}$	0.999 (0.718)
Overall *B* factor from Wilson plot (Å^2)	23.7

Table 2
Structure solution and refinement.

Values in parentheses are for the outer shell.

Resolution range (Å)	19.7–1.65
Completeness (%)	99.6
σ Cutoff	None
No. of reflections, working set	76921
No. of reflections, test set	5634
Final $R_{\rm cryst}$	0.208
Final $R_{\rm free}$	0.222
No. of non-H atoms	
Protein	4307
Ion	10
Ligand	68
Water	221
Total	4606
R.m.s. deviations	
Bonds (Å)	0.008
Angles (°)	1.308
Average *B* factors (Å^2)	
Protein	35.4
Ion	47.6
Ligand	31.4
Water	35.2
Ramachandran plot	
Most favoured (%)	99.0
Allowed (%)	1.0

co-expression construct to ensure complete dephosphorylation of FGFR1 to produce a homogeneous sample suitable for crystallization. The N-terminally His-tagged FGFR1 protein was produced by transformation into *E. coli* BL21 (DE3) cells and expression in 500 ml Terrific Broth medium supplemented with 50 mg ml^{-1} ampicillin and incubated with shaking (180 rev min^{-1}) at 310 K until the culture reached an OD_{600} of 0.7–1.0. The culture was transferred to an incubator at 291 K for 30 min before induction with 1 m*M* IPTG and was incubated for 18 h with shaking (180 rev min^{-1}) before harvesting the cells.

The cells were harvested by centrifugation at 6000*g* for 30 min at 277 K and were resuspended in Ni buffer *A* [20 m*M* Tris–HCl pH 7.8, 10 m*M* imidazole, 300 m*M* NaCl, 2 m*M* TCEP supplemented with 1× cOmplete EDTA-free protease-inhibitor tablet (Roche) per 50 ml volume]. The resuspended pellet was lysed by cell disruption (18 MPa) and the lysate was cleared by centrifugation at 20 000*g* for 30 min at 277 K. The supernatant was applied onto a 5 ml HiTrap immobilized metal (Ni^{2+}) affinity chromatography (IMAC) column (GE Healthcare) pre-equilibrated with Ni buffer *A* and was eluted using a linear gradient of Ni buffer *B* (20 m*M* Tris–HCl pH 7.8, 500 m*M* imidazole, 300 m*M* NaCl, 2 m*M* TCEP). Protein-containing fractions were pooled and dialysed against dialysis buffer (20 m*M* Tris–HCl pH 7.8, 20 m*M* NaCl, 2 m*M* TCEP) overnight at 277 K with the addition of recombinant *Tobacco etch virus* (rTEV) protease. The protein was then subjected to a second IMAC step to remove His-tagged rTEV protease, cleaved His tag and uncleaved His-tagged FGFR1.

Cleaved FGFR1 was subjected to an anion-exchange chromatography step by loading the flowthrough from the second IMAC step directly onto a 5 ml HiTrap QFF column (GE Healthcare) pre-equilibrated with QFF buffer *A* (20 m*M* Tris–HCl pH 7.8, 20 m*M* NaCl, 5 m*M* EDTA, 2 m*M* TCEP) and eluting the protein with a linear NaCl gradient using QFF buffer *B* (20 m*M* Tris–HCl pH 7.8, 1.0 M NaCl, 5 m*M* EDTA, 2 m*M* TCEP). The eluted protein was pooled, buffer-exchanged using QFF buffer *A* and finally concentrated to 40 mg ml^{-1} using a 30 kDa molecular-weight spin column (Millipore). The purified protein was made up to 50% glycerol and stored at 253 K.

2.2. Crystallization and data collection

FGFR1 protein was thawed and buffer-exchanged to remove glycerol before being diluted to 7.5 mg ml^{-1} and being incubated on ice with AZD4547 (LC Laboratories, Woburn, Massachusetts, USA; catalogue No. A-1088) in a twofold molar excess with respect to the protein. The protein complex was subjected to hanging-drop vapour diffusion: a 1 µl volume of protein–AZD4547 was mixed on a siliconized glass cover slip with 1 µl crystallization solution comprising 20% MPEG 5000, 0.25 *M* ammonium sulfate, 0.1 *M* sodium cacodylate and the cover slip was inverted over a 500 µl reservoir. The drop was left to equilibrate overnight at 291 K before streak-seeding with previously grown uncomplexed FGFR1 crystals. Large, well diffracting crystals appeared within two weeks. The crystals were cryoprotected in a 70:30 Paratone:mineral oil mixture before flash-cooling in liquid nitrogen. Diffraction data were collected on the MX2 beamline at the Australian Synchrotron (AS) using the *Blu-Ice* software (McPhillips *et al.*, 2002). The data were processed using *XDS* (Kabsch, 2010), *POINTLESS* and *AIMLESS* (Evans & Murshudov, 2013). Table 1 lists the data-collection statistics.

2.3. Structure determination, refinement and analysis

The structure of the complex was solved by molecular replacement in space group *C*2 using *Phaser* (McCoy *et al.*, 2007) and the coordinates of PDB entry 1fgi (Mohammadi *et al.*, 1997). Two protein chains were refined using a maximum-

likelihood method in *REFMAC* (Murshudov *et al.*, 2011) and the resulting structure was manually fitted and refined by real-space refinement using *Coot* (Emsley *et al.*, 2010). Residual electron density was observed in the ATP-binding site of both proteins and could be unambiguously fitted with the AZD4547 molecule generated using the ligand-building feature of *Coot*. Two AZD4547 molecules were included in the *REFMAC* refinement; iterative rounds of modelling and refinement allowed the inclusion of 221 water molecules and two sulfate anions in the structural model. The structure was assessed for completeness and quality using *MolProbity* (Chen *et al.*, 2010) and the PDB validation tools. Final refinement statistics are included in Table 2.

Coordinates and structure factors have been deposited in the PDB as entry 4wun.

3. Results and discussion

3.1. Structure determination and model quality

The kinase domain of FGFR1 was produced by co-expression with the phosphatase PTP1B and was crystallized in space group *C*2 following a standard literature protocol (Guagnano *et al.*, 2011) with minor modifications. Co-expression with the phosphatase and the replacement of two cysteine residues from wild-type FGFR1, result in a homogeneous un-phosphorylated sample suitable for crystallographic studies and no disulfide-mediated aggregation of the protein during purification. The structure of the AZD4547–FGFR1 complex was solved by molecular replacement to a resolution of 1.65 Å and contains two molecules of the protein, displaying the canonical two-lobe structure of the FGFR1 kinase domain (Fig. 2). Key features of the kinase domain are indicated in Fig. 2, including the 'hinge' region (Glu562–Lys566) about which the two N-terminal and C-terminal lobes can rotate relative to each other during ligand binding and catalysis, the 'P-loop' (Lys482–Leu494) that wraps over ATP during catalysis and the αC helix and DFG motif that are indicative of the active/inactive conformation of protein kinases. The protein was modelled in chain *A* from Leu464 to Glu765 with internal regions of disorder or unclear electron density not fitted (Gly580, Ala645–Leu662 and Phe710); chain *B* was similarly modelled over the residue range Ser461–Ser762 with some internal sections not modelled (Asp501–Asp503, Gly580–Glu593 and Arg646–Arg661). The most extensive 'missing' region in both molecules *A* and *B* is the activation loop immediately after the DFG motif. The two proteins in the asymmetric unit are very similar when overlaid, with an overall r.m.s. deviation of 0.66 Å over 260 C^{α} coordinates. A molecule of AZD4547 is located in each ATP-binding site in an unambiguous location and orientation and restrained to the 3*R*,5*S* configuration of the dimethyl piperazine N atoms (Figs. 2 and 3*a*). While both ligands bind in an equivalent manner, the protein model around the AZD4547 molecule from chain *B* is more clearly defined than that from chain *A* and so this model will be discussed from here on. The structure also contains two loosely bound surface sulfate anions and 221 water molecules. The model displays an R_{work} of 20.8% and an R_{free} of 22.2%, an r.m.s. deviation in bond lengths of 0.008 Å and an r.m.s. deviation in bond angles of 1.308°, and with 99% of the backbone torsion angles in the most favoured conformation and the remaining 1% in allowed conformations. The *MolProbity* score for the protein was assessed to be 100% compared with models of similar resolution.

3.2. Molecular recognition between AZD4547 and FGFR1

The protein in the current structure adopts an active kinase conformation displaying the characteristic 'DFG-in' conformation (Nagar *et al.*, 2002) and an intact hydrophobic spine (Kornev *et al.*, 2006). The AZD4547 molecule is located in the ATP-binding site, and consistent with the active kinase conformation of the protein, can be characterized as a type I

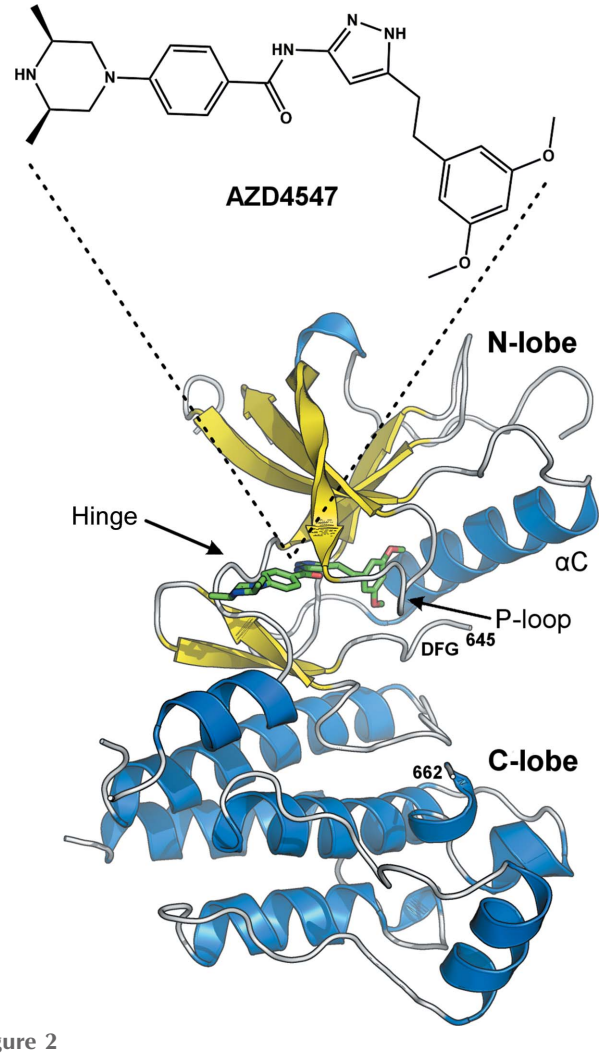

Figure 2
Structure of the AZD4547–FGFR1 kinase complex. The protein is shown in ribbon representation with α-helices coloured blue and β-sheets coloured yellow. The N-terminal lobe, C-terminal lobe, the hinge region between the lobes, the αC helix and the location of the DFG motif are indicated. Following the DFG motif, the activation loop is not modelled between residues Ala645 and Leu662, as indicated. The AZD4547 molecule binds in the ATP pocket and is shown as a green stick model. This figure was drawn using *PyMOL* (Schrödinger).

kinase inhibitor. A survey of the current FGFR1–inhibitor entries in the PDB shows that these inhibitors, whether FGFR1-selective or not, all bind in a type I mode. This ATP-competitive binding mode, given the conservation of the ATP-pocket across the kinase family, is generally not selective, with a broad kinase hit range (reviewed by Garuti *et al.*, 2010; Blanc *et al.*, 2013).

The AZD4547 molecule is bound deeply into the ATP-binding cavity, forming three hydrogen bonds to the hinge region of the protein (Fig. 3*b*), specifically between N2 and Ala564 O (3.1 Å), between N4 and Ala564 N (3.0 Å) and between N3 and Glu562 O (2.9 Å). A hydrogen bond is also formed from the dimethoxyphenyl ring O1 atom to the C-terminal lobe atom Asp641 N (2.9 Å). The P-loop wraps closely over the AZD4547 molecule, is well ordered and in the process traps three water molecules (Fig. 3*c*) that form an ordered solvent network linking the P-loop and the AZD4547 carbonyl O atom through hydrogen bonding in chain *B*. This water network is not well ordered in chain *A* and is modelled with two waters removed. The trapped water molecules forming a hydrogen-bond network to AZD4547 in chain *B* may not be a critical determinant of the inhibitor binding affinity; solvent space remains to be filled in chain *A*, albeit by disordered water molecules. The AZD4547 molecule makes a total of 41 van der Waals contacts with the protein structure (<3.8 Å) as shown schematically in Fig. 3(*c*) (the full list of contacts is included in the Supporting Information).

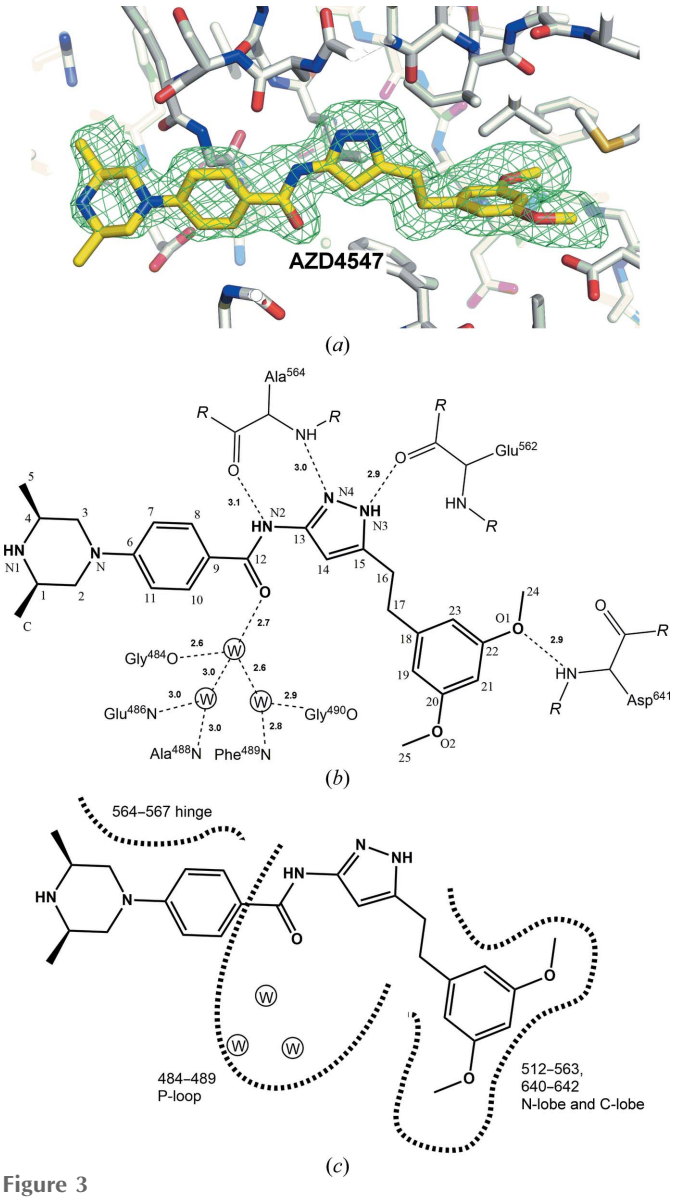

Figure 3
Binding of AZD4547 in the ATP pocket of FGFR1. (*a*) $F_o - F_c$ electron-density map (scaled to 2.5σ in *PyMOL*) surrounding the AZD4547 molecule before the inhibitor was included in refinement. The inhibitor could be fitted unambiguously in the electron density. (*b*) Schematic showing hydrogen-bonding interactions and distances in Å between AZD4547 and the protein structure and including a water network trapped inside the P-loop. This figure was drawn using *ChemDraw*. (CambridgeSoft). (*c*) Schematic showing regions of the protein involved in van der Waals interactions with AZD4547. This figure was drawn using *ChemDraw*.

The dimethoxyphenyl to pyrazole region of the AZD4547 molecule binds in a mode very similar to that of pyrazol-aminopyrimidine **1** (Figs. 1, 4*a* and 4*b*) from PDB entry 4nk9 (Klein *et al.*, 2013) with the same hydrogen-bond interactions formed to the hinge region of the protein. In both cases the well overlaid dimethoxyphenyl rings bind deep in a pocket surrounded by numerous hydrophobic residues. However, while for pyrazolaminopyrimidine **1** the positively charged side-chain terminus of Lys514 forms a π–cation interaction over the centre of the dimethoxyphenyl ring, the equivalent location in the AZD4547 structure contains a water molecule (W80) hydrogen-bonded between Lys514 NZ and Glu531 OE2. In this AZD4547 binding mode the side chains of Lys514 and Asp641 are pushed out of the pocket by the close approach of the Phe489 side chain at the tip of the P-loop that has closely wrapped over the ligand. The Phe489 side-chain location and the trapped water network of the current structure is occupied by the ligand in the 4nk9 structure (Fig. 4*b*); in the AZD4547 structure the remainder of the inhibitor molecule 'hugs' the hinge region of the protein and extends towards solvent.

3.3. The P-loop and cavity formation

A defining structural feature of the AZD4547 binding mode is the tight closure of the P-loop over the inhibitor molecule and its highly kinked conformation. Is the P-loop closure an effect of ligand binding or a crystal-packing artefact? While there is a close contact (crystal packing) between the P-loop in chain *B* and an adjacent molecule (Glu486 O–Pro579 $-x - 1/2, y - 1/2, -z + 1$; 3.2 Å), the P-loop in chain *A* is not involved in crystal-packing interactions at all (the closest approach is 11 Å) and both loops have near-identical conformations, with an r.m.s. deviation of 0.19 Å over all 64 main-chain atoms of the section Leu480–Ala495 when overlaid. This suggests that the unusual conformation of the P-loop is attained in solution and that the crystal packing has not dictated the protein conformation in the current co-crystals. The unliganded FGFR1 protein in PDB entry 1fgk (Mohammadi *et al.*, 1997) shows an open conformation of the P-loop,

further implicating the AZD4547 ligand binding in the extreme P-loop closure observed.

The P-loop closure is promoted by the elongated and narrow scaffold of AZD4547, allowing a close approach of this

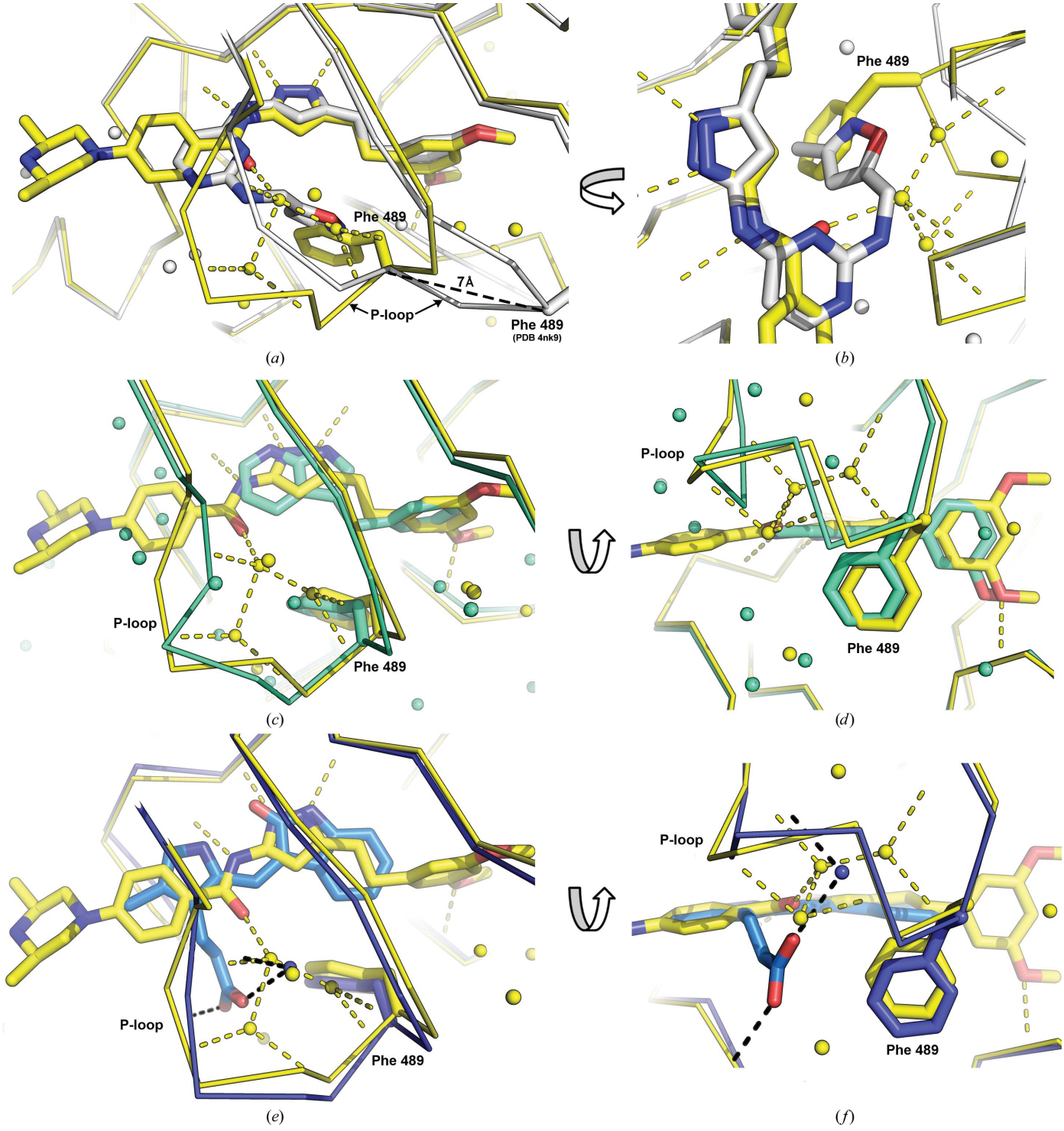

Figure 4
Comparison of the AZD4547, 4nk9, 3c4f and 1fgi structures. (*a*) Top view of overlaid AZD4547 and 4nk9 structures showing similarities in chemical scaffold at the right-hand end of the two inhibitor molecules. The AZD4547 structure is coloured yellow and the 4nk9 structure white. The ligands are drawn as stick models and water molecules as small spheres. Hydrogen bonds are indicated by dashed yellow lines and are shown for the AZD4547 structure only for clarity. The P-loop of the current structure is shifted approximately 7 Å at Phe489 compared with the 4nk9 structure and adopts a very different conformation. The side-chain location of Phe489 in the current structure would clash with the 4nk9 inhibitor. (*b*) Side view of an AZD4547/4nk9 overlay. (*c*) Top view and (*d*) front view of AZD4547 (yellow) and 3c4f (green) superimposition. (*e*) Top view and (*f*) front view of AZD4547 (yellow) and 1fgi (blue) superimposition. Hydrogen bonding for AZD4547 is depicted as yellow dashed lines, while the hydrogen bonding of the 1fgi inhibitor between its carboxylate side chain and the protein P-loop and C-lobe is shown as black dashed lines. These figures were drawn using *PyMOL*.

loop and also the inclusion in AZD4547 of the linking amide carbonyl that forms a hydrogen-bond network with the trapped water molecules described above stabilizing the loop structure. This loop closure and the trapped water molecules form a long and tight hydrophobic pocket creating extensive van der Waals interactions with the inhibitor, from which only the dimethyl piperazine ring protrudes (Figs. 5*b* and 5*c*). The extent of this pocket is further illustrated in the cross-sections depicted in Figs. 5(*d*) and 5(*e*). The burial of Phe489 to form new van der Waals interactions with both the inhibitor (primarily with AZD4547 atom C17) and protein (Leu630, Arg627, Asn628 and Ala640 residues), and its exclusion from aqueous solvent, appears to provide a significant stabilizing force for the closed structure.

This loop closure is more pronounced than nearly all other reported FGFR1 structures, including ATP-bound and inhibitor-bound structures, but is remarkably similar to the loop configuration of the two inhibitor structures PDB entries 3c4f (Tsai *et al.*, 2008) and 1fgi (Mohammadi *et al.*, 1997). Are there any common features between AZD4547 and the two inhibitors from these structures? The molecule 3-(3-methoxybenzyl)-1*H*-pyrrolo[2,3-b]pyridine (**2**; Fig. 1) in structure 3c4f is small in size, overlays AZD4547 closely and displays a similar hydrogen-bonding pattern to the hinge-region backbone and through the single methoxy substituent to Asp641 N as we observe for AZD4547 (Figs. 4*c* and 4*d*). The molecule SU4502 (Fig. 1) in the 1fgi structure again overlays AZD4547 but does not bind into the hydrophobic pocket used by the AZD4547 dimethoxyphenyl ring (Figs. 4*e* and 4*f*). It is also a relatively narrow molecule and hydrogen-bonds into the hinge region backbone in the same location as AZD4547. The carboxylate side chain of SU4502 extends into the area occupied by the trapped water molecules surrounding the P-loop in the current structure and clearly stabilizes the closed loop structure of 1fgi through hydrogen bonding.

A closer inspection of the closed loop in the AZD4547 structure suggests a unique stabilizing interaction (Fig. 6). The loop closure and the reorientation of the Lys514 side chain forms a strong hydrogen bond/electrostatic link from Phe489 O to Lys514 NZ and then to Glu531 OE1. In addition, the water molecule (W80) which π-stacks with the dimethoxyphenyl ring also bridges the loop residue Phe489 and Glu531 from the N-lobe by hydrogen bonding and makes an interaction with Lys514 NZ. This network of interactions contributes to the configuration and stability of the P-loop and allows the burial of hydrophobic features of both the loop and ligand and the formation of the network of trapped waters linking the P-loop to AZD4547 as described above.

What is the significance of the observed P-loop closure; does this confer or contribute significantly to the high binding affinity or, perhaps more importantly, to the selectivity for FGFR proteins of AZD4547? If we consider the two structures with PDB codes 3c4f

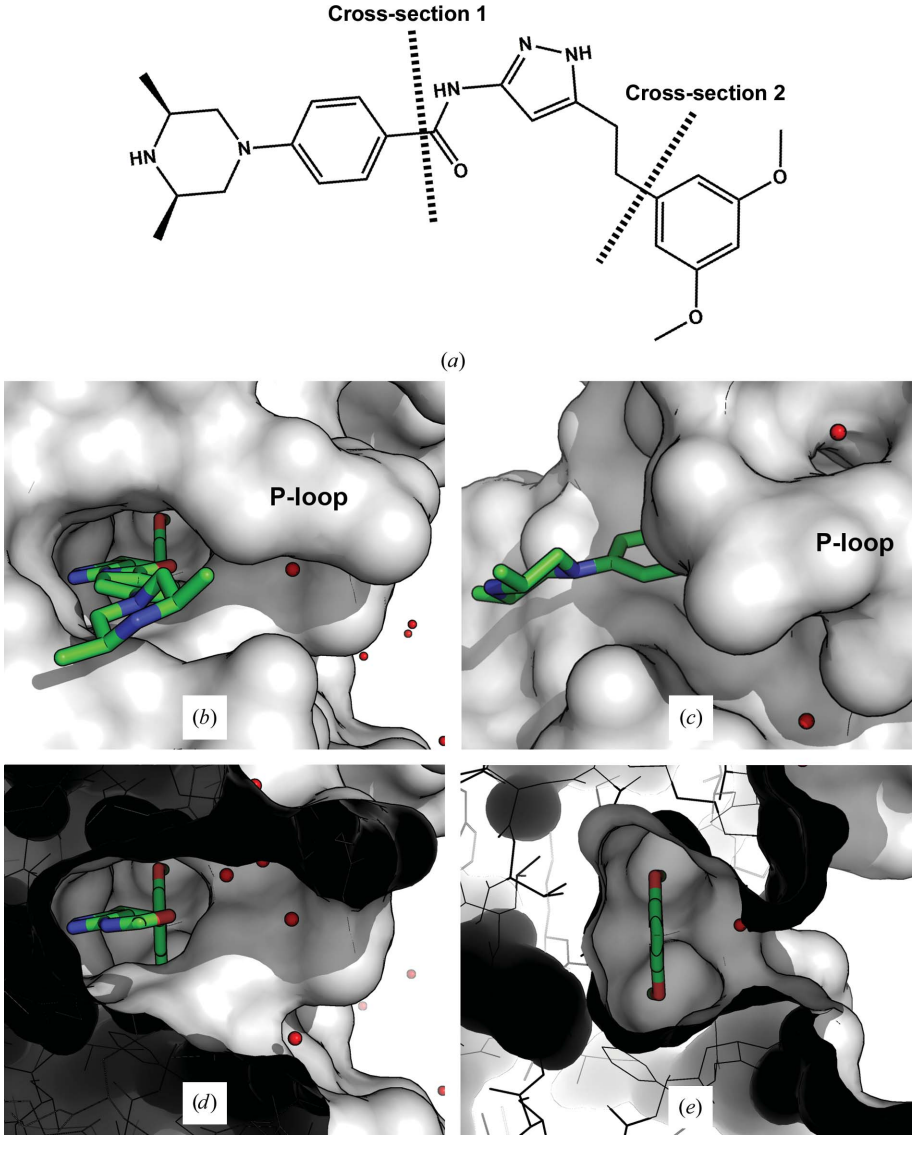

Figure 5
Surface of the AZD4547–FGFR1 complex. (*a*) Schematic of AZD4547 showing the location of the cross-section points illustrated below. (*b*) Side view of the long, narrow AZD4547 binding pocket formed by the closure of the P-loop. Water molecules are indicated by red spheres and were not included in the protein surface calculation. (*c*) Front view of a surface illustration showing the extent of AZD4547 burial by the P-loop. (*d*) Cross-section 1 as indicated in (*a*); the trapped water molecules fill the space between the inhibitor and the extent of the P-loop. (*e*) Cross-section 2; the dimethoxyphenyl ring is shown deeply buried in a hydrophobic pocket with a water molecule π-stacked over the centre of the aromatic ring. These figures were drawn using *PMOL*.

and 1fgi described above, the SU4502 molecule is a 30 n*M* (IC_{50}) inhibitor of FGFR1, but 3-(3-methoxybenzyl)-1*H*-pyrrolo[2,3-b]pyridine is a much less potent inhibitor, with an IC_{50} of 2 μ*M*; we have found no information relating to kinase selectivity for these compounds. However, we find support for P-loop closure as a selectivity mechanism in other kinase systems, as reviewed by Guimarães *et al.* (2011). This statistical and computational analysis of kinase crystal structures shows that the extreme P-loop closure, or folded conformation, is rare, with a prevalence of only 12.5% in a database of 2690 kinase–ligand structures. Examples of this P-loop conformation are found in Abl, ACK1, AURA, cMet, FGFR1, MAP4K4 and p38 kinases, although the more extended conformation of the P-loop is far more prevalent in their liganded complexes. It appears that the P-loops of these kinases have an intrinsic ability to form the tightly folded structure but only when induced to do so by the binding of specific ligands. The computational analysis of selectivity by Guimarães and coworkers shows that 21 out of 27 systems for which suitable inhibition data were available can be considered to be examples of selective inhibition and concludes that the ability of an inhibitor to induce P-loop closure is a bone fide selectivity mechanism, particularly when the P-loop Phe or Tyr residue makes direct contacts with the ligand, as we observed for FGFR1 Phe489 and AZD4547. The conformation and flexibility of the P-loop in Abl kinase has been studied quite extensively, and in relation to imatinib binding a folded P-loop conformation is observed and correlates with the occurrence of clinically observed imatinib mutations in the protein P-loop that are likely to disrupt the hydrophobic cage around the inhibitor (Hari *et al.*, 2013; Deininger *et al.*, 2005). Other biochemical and structural studies have suggested that a major contribution to the selectivity of imatinib for Abl over Src kinase derives specifically from the interaction between the flexible Abl P-loop and the inhibitor (Dar *et al.*, 2008; Seeliger *et al.*, 2009).

Our structure shows AZD4547 to be a type 1 kinase inhibitor targeting the active kinase conformation of FGFR1 and we cannot point to specific features of the observed binding mode that would confer the high level of selectivity for FGFR1. Indeed, it is a general observation that type 1 kinase inhibitors are not selective inhibitors and hit many off-targets. Nevertheless, there is a compelling argument to be made that the induction of a folded P-loop conformation is an important component of AZD4547 selectivity, although this putative mechanism may be difficult to rationally design into novel inhibitors. The structure of AZD4547 bound to FGFR1 displays what might be described as an example of exquisite molecular recognition between an inhibitor and protein and highlights an elegant and successful structure-guided drug-discovery process by AstraZeneca to produce a selective subnanomolar inhibitor of FGFR1.

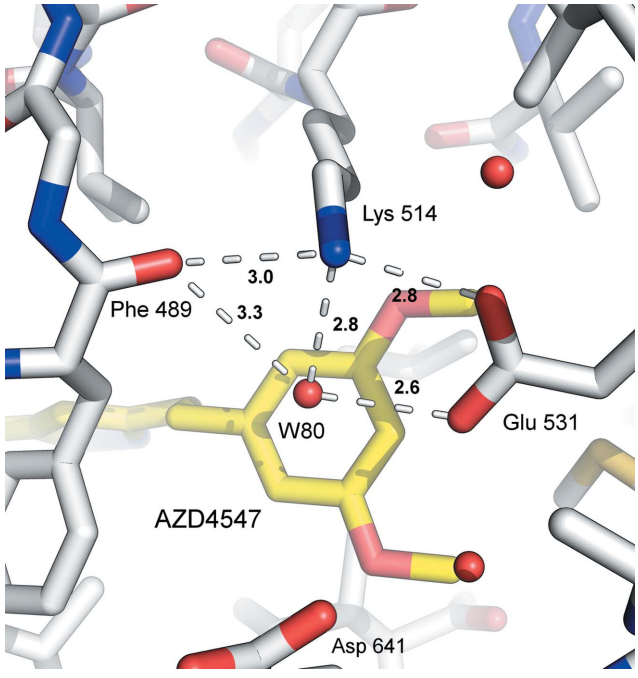

Figure 6
Interactions stabilizing the P-loop closure in the AZD4547 structure. The FGFR1 protein is drawn as a stick model with C atoms coloured white; the AZD4547 molecule is coloured yellow. Water molecules are shown as small red spheres and hydrogen-bonding interactions as white dashed lines with distances labelled in Å. This figure was drawn using *PyMOL*.

Acknowledgements

We acknowledge the Health Research Council of New Zealand for funding support (HRC 13/196). This research was undertaken on the MX2 beamline at the Australian Synchrotron, Victoria, Australia.

References

Armstrong, K., Ahmad, I., Kalna, G., Tan, S. S., Edwards, J., Robson, C. N. & Leung, H. Y. (2011). *Br. J. Cancer*, **105**, 1362–1369.
Beenken, A. & Mohammadi, M. (2009). *Nature Rev. Drug Discov.* **8**, 235–253.
Blanc, J., Geney, R. & Menet, C. (2013). *Anticancer Agents Med. Chem.* **13**, 731–747.
Brooks, A. N., Kilgour, E. & Smith, P. D. (2012). *Clin. Cancer Res.* **18**, 1855–1862.
Cappellen, D., De Oliveira, C., Ricol, D., de Medina, S., Bourdin, J., Sastre-Garau, X., Chopin, D., Thiery, J. P. & Radvanyi, F. (1999). *Nature Genet.* **23**, 18–20.
Chen, V. B., Arendall, W. B., Headd, J. J., Keedy, D. A., Immormino, R. M., Kapral, G. J., Murray, L. W., Richardson, J. S. & Richardson, D. C. (2010). *Acta Cryst.* D**66**, 12–21.
Chou, T. & Finn, R. S. (2012). *Future Oncol.* **8**, 1083–1090.
Dar, A. C., Lopez, M. S. & Shokat, K. M. (2008). *Chem. Biol.* **15**, 1015–1022.
Deininger, M., Buchdunger, E. & Druker, B. J. (2005). *Blood*, **105**, 2640–2653.
Dieci, M. V., Arnedos, M., Andre, F. & Soria, J. C. (2013). *Cancer Discov.* **3**, 264–279.
Emsley, P., Lohkamp, B., Scott, W. G. & Cowtan, K. (2010). *Acta Cryst.* D**66**, 486–501.
Eswarakumar, V. P., Lax, I. & Schlessinger, J. (2005). *Cytokine Growth Factor Rev.* **16**, 139–149.
Evans, P. R. & Murshudov, G. N. (2013). *Acta Cryst.* D**69**, 1204–1214.
Garuti, L., Roberti, M. & Bottegoni, G. (2010). *Curr. Med. Chem.* **17**, 2804–2821.

Gavine, P. R., Mooney, L., Kilgour, E., Thomas, A. P., Al-Kadhimi, K., Beck, S., Rooney, C., Coleman, T., Baker, D., Mellor, M. J., Brooks, A. N. & Klinowska, T. (2012). *Cancer Res.* **72**, 2045–2056.
Guagnano, V. *et al.* (2011). *J. Med. Chem.* **54**, 7066–7083.
Guagnano, V. *et al.* (2012). *Cancer Discov.* **2**, 1118–1133.
Guimarães, C. R., Rai, B. K., Munchhof, M. J., Liu, S., Wang, J., Bhattacharya, S. K. & Buckbinder, L. (2011). *J. Chem. Inf. Model.* **51**, 1199–1204.
Hari, S. B., Perera, B. G., Ranjitkar, P., Seeliger, M. A. & Maly, D. J. (2013). *ACS Chem. Biol.* **8**, 2734–2743.
Hart, K. C., Robertson, S. C., Kanemitsu, M. Y., Meyer, A. N., Tynan, J. A. & Donoghue, D. J. (2000). *Oncogene*, **19**, 3309–3320.
Hilberg, F., Roth, G. J., Krssak, M., Kautschitsch, S., Sommergruber, W., Tontsch-Grunt, U., Garin-Chesa, P., Bader, G., Zoephel, A., Quant, J., Heckel, A. & Rettig, W. J. (2008). *Cancer Res.* **68**, 4774–4782.
Kabsch, W. (2010). *Acta Cryst.* D**66**, 125–132.
Kasper, B. & Hohenberger, P. (2011). *Future Oncol.* **7**, 1373–1383.
Kim, K. B., Chesney, J., Robinson, D., Gardner, H., Shi, M. M. & Kirkwood, J. M. (2011). *Clin. Cancer Res.* **17**, 7451–7461.
Klein, T., Tucker, J., Holdgate, G. A., Norman, R. A. & Breeze, A. L. (2013). *ACS Med. Chem. Lett.* **5**, 166–171.
Klint, P. & Claesson-Welsh, L. (1999). *Front. Biosci.* **4**, 165–177.
Kornev, A. P., Haste, N. M., Taylor, S. S. & Ten Eyck, L. F. (2006). *Proc. Natl Acad. Sci. USA*, **103**, 17783–17788.
Ledermann, J. A., Hackshaw, A., Kaye, S., Jayson, G., Gabra, H., McNeish, I., Earl, H., Perren, T., Gore, M., Persic, M., Adams, M., James, L., Temple, G., Merger, M. & Rustin, G. (2011). *J. Clin. Oncol.* **29**, 3798–3804.
Liang, G., Liu, Z., Wu, J., Cai, Y. & Li, X. (2012). *Trends Pharmacol. Sci.* **33**, 531–541.
McCoy, A. J., Grosse-Kunstleve, R. W., Adams, P. D., Winn, M. D., Storoni, L. C. & Read, R. J. (2007). *J. Appl. Cryst.* **40**, 658–674.
McPhillips, T. M., McPhillips, S. E., Chiu, H.-J., Cohen, A. E., Deacon, A. M., Ellis, P. J., Garman, E., Gonzalez, A., Sauter, N. K., Phizackerley, R. P., Soltis, S. M. & Kuhn, P. (2002). *J. Synchrotron Rad.* **9**, 401–406.
Mohammadi, M., Froum, S., Hamby, J. M., Schroeder, M. C., Panek, R. L., Lu, G. H., Eliseenkova, A. V., Green, D., Schlessinger, J. & Hubbard, S. R. (1998). *EMBO J.* **17**, 5896–5904.
Mohammadi, M., McMahon, G., Sun, L., Tang, C., Hirth, P., Yeh, B. K., Hubbard, S. R. & Schlessinger, J. (1997). *Science*, **276**, 955–960.
Mohammadi, M., Olsen, S. K. & Ibrahimi, O. A. (2005). *Cytokine Growth Factor Rev.* **16**, 107–137.
Murshudov, G. N., Skubák, P., Lebedev, A. A., Pannu, N. S., Steiner, R. A., Nicholls, R. A., Winn, M. D., Long, F. & Vagin, A. A. (2011). *Acta Cryst.* D**67**, 355–367.
Nagar, B., Bornmann, W. G., Pellicena, P., Schindler, T., Veach, D. R., Miller, W. T., Clarkson, B. & Kuriyan, J. (2002). *Cancer Res.* **62**, 4236–4243.
Nieto, M., Borregaard, J., Ersboll, J., ten Bosch, G. J., van Zwieten-Boot, B., Abadie, E., Schellens, J. H. & Pignatti, F. (2011). *Clin. Cancer Res.* **17**, 6608–6614.
Norman, R. A., Schott, A. K., Andrews, D. M., Breed, J., Foote, K. M., Garner, A. P., Ogg, D., Orme, J. P., Pink, J. H., Roberts, K., Rudge, D. A., Thomas, A. P. & Leach, A. G. (2012). *J. Med. Chem.* **55**, 5003–5012.
Pardo, O. E., Arcaro, A., Salerno, G., Raguz, S., Downward, J. & Seckl, M. J. (2002). *J. Biol. Chem.* **277**, 12040–12046.
Pardo, O. E., Lesay, A., Arcaro, A., Lopes, R., Ng, B. L., Warne, P. H., McNeish, I. A., Tetley, T. D., Lemoine, N. R., Mehmet, H., Seckl, M. J. & Downward, J. (2003). *Mol. Cell. Biol.* **23**, 7600–7610.
Pardo, O. E., Wellbrock, C., Khanzada, U. K., Aubert, M., Arozarena, I., Davidson, S., Bowen, F., Parker, P. J., Filonenko, V. V., Gout, I. T., Sebire, N., Marais, R., Downward, J. & Seckl, M. J. (2006). *EMBO J.* **25**, 3078–3088.
Ray-Coquard, I. & Thomas, D. (2012). *Nature Rev. Clin. Oncol.* **9**, 431–432.
Seeliger, M. A., Ranjitkar, P., Kasap, C., Shan, Y., Shaw, D. E., Shah, N. P., Kuriyan, J. & Maly, D. J. (2009). *Cancer Res.* **69**, 2384–2392.
Sharpe, R., Pearson, A., Herrera-Abreu, M. T., Johnson, D., Mackay, A., Welti, J. C., Natrajan, R., Reynolds, A. R., Reis-Filho, J. S., Ashworth, A. & Turner, N. C. (2011). *Clin. Cancer Res.* **17**, 5275–5286.
Tsai, J. *et al.* (2008). *Proc. Natl Acad. Sci. USA*, **105**, 3041–3046.
Turner, N. & Grose, R. (2010). *Nature Rev. Cancer*, **10**, 116–129.
Weiss, J. *et al.* (2012). *Sci. Transl. Med.* **2**, 62ra93.
Zhang, X., Ibrahimi, O. A., Olsen, S. K., Umemori, H., Mohammadi, M. & Ornitz, D. M. (2006). *J. Biol. Chem.* **281**, 15694–15700.
Zhou, W., Hur, W., McDermott, U., Dutt, A., Xian, W., Ficarro, S. B., Zhang, J., Sharma, S. V., Brugge, J., Meyerson, M., Settleman, J. & Gray, N. S. (2010). *Chem. Biol.* **17**, 285–295.